Hindawi
Advances in Polymer Technology
Volume 2019, Article ID 8482975, 12 pages
https://doi.org/10.1155/2019/8482975

Research Article

Synthesis of Poly(AN-co-VP)/Zeolite Composite and Its Application for the Removal of Brilliant Green by Adsorption Process: Kinetics, Isotherms, and Experimental Design

Mehtap Tanyol,[1] **Nevroz Kavak**,[1] **and Gülben Torğut**[2]

[1]*Munzur University, Department of Environmental Engineering, Tunceli, Turkey*
[2]*Munzur University, Vocational School of Tunceli, Department of Chemistry and Chemical Processes, Tunceli, Turkey*

Correspondence should be addressed to Mehtap Tanyol; mtanyol@munzur.edu.tr

Received 23 October 2018; Revised 15 November 2018; Accepted 18 December 2018; Published 3 January 2019

Academic Editor: Sébastien Déon

Copyright © 2019 Mehtap Tanyol et al. This is an open access article distributed under the Creative Commons Attribution License, which permits unrestricted use, distribution, and reproduction in any medium, provided the original work is properly cited.

In this study, a poly(acrylonitrile-co-N-vinyl pyrrolidone)/zeolite (poly(AN-co-VP)/zeolite) composite was synthesized by in situ free radical polymerization (FRP). The structural properties of the composite were analyzed by Fourier transform infrared spectroscopy (FT-IR), X-ray diffraction (XRD), scanning electron microscopy (SEM), thermogravimetric analysis (TGA), and differential scanning calorimetry (DSC). The characterization results indicated that the composite had a homogeneous and 3-dimensional (3D) structure. The decomposition temperature and glass transition temperature (T_g) were found as 410°C and 152°C, respectively. A poly(AN-co-VP)/zeolite composite was used to investigate the adsorption of brilliant green (BG) which is a water-soluble cationic dye. The kinetics, isotherms, and thermodynamics of adsorption were examined, and results showed that equilibrium data fitted the Langmuir isotherm model, and the adsorption kinetics of BG followed pseudo-second-order model. According to the thermodynamic properties, the adsorption process was endothermic and spontaneous. Response surface methodology (RSM), which was improved by the application of the quadratic model associated with the central composite design, was employed for the optimization of the study conditions such as adsorbent mass, time, and initial dye concentration. The RSM indicated that maximum BG removal (99.91%) was achieved at the adsorbent mass of 0.20 g/50 mL, an initial BG concentration of 40.20 mg/L, and a contact time of 121.60 minutes.

1. Introduction

Water pollution, which is one of the most unfavorable environmental problems in the world, stems from many reasons. One of these is synthetic dyes colored organic substances that cause irritation of the skin, mutagenicity, carcinogenicity, and damage to aquatic life [1–3]. Brilliant green (BG), commonly known as cationic dye, is one of the most important dyes and is extensively used as a dyeing agent in industries such as paper printing, wood, and textile. BG, which is from the triphenylmethane dye family, is very dangerous in case of contact with the skin and eyes and toxic to the lungs. It is very important to remove BG from aqueous solutions due to the formation of carbon dioxide, sulfur oxides, and nitrogen oxides during its decomposition [4–7]. It is a very difficult process to treat the dyes because they are not biodegradable and they have a highly complex aromatic molecular structure that makes them more stable [8].

There are many different physical, chemical, and biological techniques that can be used to remove dyes from water. Among them adsorption is a viable alternative method in the removal of contaminants from wastewaters due to its major advantages such as high efficiency, easy application, design simplicity, low cost, specific interactions between solid adsorbent molecules and dyes, and insensitivity to toxic pollutant [9, 10]. In addition, the main advantage of adsorption is that many natural and inexpensive materials such as natural materials, biosorbents, and solid wastes from industry and agriculture can be used as an adsorbent without any complicated equipment [11–13].

In recent years, the preparation of organic–inorganic composites has become a focus of interest due to their low

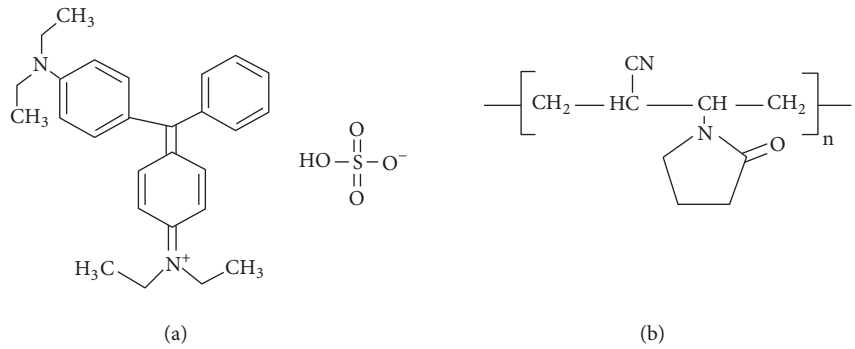

(a) (b)

Scheme 1: Chemical structure of (a) BG and (b) poly(AN-co-VP).

production cost and higher mechanical resistance, and thus they have been used for the adsorption of dyes. Different kinds of substances such as montmorillonite, activated clay, bentonite, zeolite, and kaolinite have been used to form composites. These clays incorporated into the polymer increase the adsorption capacity as well as the adsorption rate [14, 15]. Zeolites are natural components which are alternatively used to form the composite with polymers [1].

Poly 1-vinyl-2-pyrrolidone is used in many applications due to its numerous unique properties such as solubility in water, hydrophilic and biocompatible properties, dispersion, and adhesion. It is also interesting because poly(vinylpyrrolidone) (PVP) is nontoxic and biological inertness [16–18].

Poly(AN-co-VP)/zeolite) composite has not been synthesized previously. However, there are some studies about synthesis of AN-co-VP copolymer. This copolymer was used for many purposes. For example, Staufenbiel et al. [19] synthesized a series of poly(acrylonitrile-co-N-vinyl-2-pyrrolidone) model nanoparticles to expand the set of model nanoparticles available for mechanistic studies of protein adsorption beyond polystyrene based lattices. Wan et al. [20] have used the poly(acrylonitrile-co-N-vinyl-2-pyrrolidone) for determining the total water content adsorbed on the PANCNVP film by swelling experiments performed at temperatures of interest. A series of rigid poly[acrylonitrile-co-(N-vinyl pyrrolidone)] model nanoparticles stably loaded with Nile Red or Rhodamine B, respectively, was comprehensively studied for biocompatibility and functionality by Zhang et al. [21]

In recent studies, a lot of adsorbents were prepared for brilliant green removal, but there are still some shortages on these adsorbents. For instance, polyaniline/silver nanocomposite was used as an adsorbent for removal of brilliant green (BG) from aqueous solutions [22]. However, the preparation of nanocomposites was probably complicated and silver is expensive. Ghaedi et al. [23] synthesized the zinc sulfide nanoparticle loaded on activated carbon and examined BG removal percentage toward various parameters including pH, adsorbent dosage, initial dye concentration, and contact time. However, this study is not very novel because activated carbon is widely used for adsorption studies due to its extremely porous and very large surface area. In our previous study, poly(AN-co-VP)/zeolite composite was prepared firstly and showed efficient adsorption ability for BG. Furthermore, this composite is generally considered to be nondegradable and thus is suitable as model systems that do not experience substantial alteration of properties in aqueous environment.

Table 1: Chemical composition of zeolite (% mass/mass).

SiO_2	Al_2O_3	FeO_3	MgO	CaO	Na_2O	K_2O	CuO
68.62	12.64	1.50	0.84	1.89	0.70	3.43	0.75

The intention of the present research is the synthesis and use of poly(AN-co-VP)/zeolite) composite to investigate the impact of three parameters: initial dye concentration, adsorbent mass, and contact time on the removal of the dye BG, using central composite design (CCD) which is a standard response surface methodology (RSM). RSM is the collection of statistical and mathematical tools and it was selected to explain the simultaneous effects of the parameters on the adsorption process [24–26].

2. Materials and Methods

2.1. Materials. Monomers (AN, VP) and the dye (BG) were supplied from Sigma-Aldrich, and they were used as received commercially. Natural zeolite was provided by a local company in Turkey. The chemical composition of the zeolite, which was analyzed by X-ray fluorescence spectrometry, was given in Table 1.

The 2,2′-azobisisobutyronitrile (AIBN) was used as an initiator. All chemicals were of analytical purity. The chemical structure of BG and copolymers of AN and VP were given in Scheme 1.

2.2. Characterization. The FT-IR spectra were recorded on a Jasco-Spectrum FT-IR spectrophotometer for the region of 4000–400 cm^{-1}. The TGA measurement was performed with a Shimadzu TGA-50 from room temperature to 500°C at a heating rate of 10°C/min. DSC analysis was recorded with a Shimadzu DSC-50 under nitrogen atmosphere from room temperature to 200°C at a heating rate of 20°C/min. Adsorption properties were examined by using a Shimadzu-1800 UV-VIS spectrophotometer. The morphology of the composite was evaluated by SEM and XRD. SEM was performed by Hitachi S-3500 with an accelerating voltage of 25 kV. The XRD spectrum was measured using an X-ray

diffractometer (Rigaku miniflex-600) at voltage 40 kV, current 15 mA.

2.3. Synthesis of the Poly(AN-co-VP)/Zeolite Composite. The poly(AN-co-VP)/zeolite composite was prepared by using in situ polymerization method. For this purpose, 2 mL of AN, 2 mL of VP monomers, and 20% by mass of zeolite were added to 4 different polymerization tubes. The mixtures were mixed in an ultrasonic bath for 1 hour. AIBN (0.03 g) was added to these mixtures and the tubes that passed through an argon gas were submerged in an oil bath previously set at 60°C. After 40 minutes the polymerization was terminated and precipitated in hexane, dried under vacuum for 24 hours.

2.4. Adsorption Studies. To examine the adsorption properties of the poly(AN-co-VP)/zeolite composite, a series of adsorption experiments were carried out. 0.2 g solid poly(AN-co-VP)/zeolite composite was mixed with different concentrations (25 mg/L-100 mg/L) of dye solution in closed erlenmeyer flasks (50 mL) at natural pH (4.5). The flasks were kept at a constant speed (300 rpm) sealed shaker to provide temperature control for different periods at a temperature of 30°C. After predetermined time intervals, the absorbance values of the solutions were measured at 625 nm by UV-VIS spectrophotometry after being centrifuged at 5000 rpm for 10 minutes. The adsorbed amount (mg/g) of BG at time t (q_t) was calculated according to (1).

$$q_t = \frac{(C_o - C_t)\,V}{m} \tag{1}$$

In addition, the adsorbed amount of BG at the equilibrium (q_e) was calculated according to

$$q_e = \frac{(C_o - C_e)\,V}{m} \tag{2}$$

where C_o, C_e, and C_t (mg/L) are the initial, equilibrium, and at any time BG concentrations, respectively. V (L) is the volume of solution, and m (mg/g) is the mass per gram of the poly(AN-co-VP)/zeolite composite.

2.5. Experimental Design with CCD. The CCD is performed to test the combined and individual effects of three independent parameters of BG adsorption process on poly(AN-co-VP)/zeolite. Adsorbent mass (A), initial BG concentration (B), and time (C) were chosen as independent parameters and the BG removal yield (%) was selected to be the response of the process (dependent parameter). A total of different experiments, including 6 axial points, 8 factorial points, and 6 replications of the central points, were performed in the five levels ($-\alpha$, -1, 0, 1, $+\alpha$) with CCD design matrix. Design Expert 7 (Stat-Ease, USA) was utilized for the evaluation of process parameters, graphical analysis, statistical analysis of the data found, and analysis of variance (ANOVA). The mathematical relationship between the process response and the three independent parameters was expressed by the following quadratic equation [33]:

$$Y\,(\%) = \beta_0 + \sum_{i=1}^{n}\beta_i x_i + \sum_{i=1}^{n}\beta_{ii}x_i^2 + \sum_{i=1}^{n-1}\sum_{j=i+1}^{n}\beta_{ij}x_i x_j \tag{3}$$

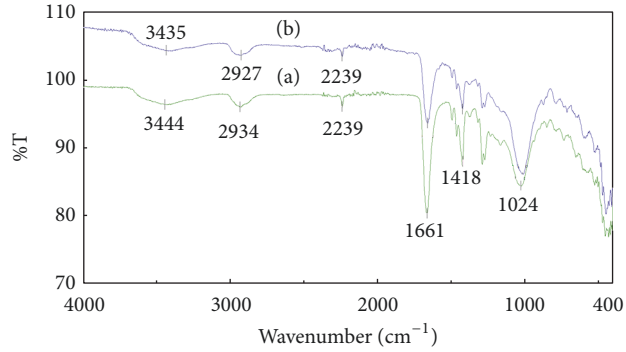

FIGURE 1: IR spectrum of the poly(AN-co-VP)/zeolite composite (a) before adsorption and (b) after adsorption.

where Y is the predicted answer (BG removal yield), β_0 is the constant coefficient, β_i is linear effects of the input variable, β_{ii} is the quadratic effects, β_{ij} is the interaction effects between the input variables, and x_i *and* x_j are the coded values of the parameters.

3. Results and Discussion

3.1. Characterization of the Poly(AN-co-VP)/Zeolite Composite. Figure 1 shows the FT-IR spectra of the poly(AN-co-VP)/zeolite composite before adsorption and after adsorption. When the spectra were compared, it was seen that there was no important change in the chemical structure of the composite after the adsorption process. This can be explained by van der Waals interaction between the dye molecules and the composite molecules and it shows that the adsorption process was carried out on the surface of the adsorbent. The peak at 3444 cm^{-1} is due to OH groups of layered alumina silicates in the zeolite. The band at 1024 cm^{-1} corresponds to Si-O-Si and Si–O–Al stretching in the zeolite. Similar results have been found in the literature [34]. 1661 cm^{-1} is the characteristic peak of the C=O stretching of the tertiary amide of VP. Also, the peak at 2239 cm^{-1} characterizes the nitrile groups (CN) on acrylonitrile units.

SEM was used for composite surface area analysis before and after BG adsorption. In Figure 2(a) the polymer surface was very rough and porous with many cavities, and when filled with BG molecules the surface was very smooth (Figure 2(b)). As a result, the morphology of the polymeric composite filled with BG demonstrates a quite difference from the pure form and indicated that the BG adsorbs more efficiently on the composite.

The crystallinity of zeolite in the poly(AN-co-VP)/zeolite composite was evaluated on the basis of the XRD background in the range $2\theta = 10$–90°. On the other hand, XRD patterns of composite consist of many sharp peaks that reflect well the crystalline structure of the system. Zeolite is characterized by many sharp peaks by XRD and they are shown in Figure 3. These peaks are clearly seen in the composite structure when compared with the literature [24]. The peaks around 11.36°, 22.47°, 30.16°, and 56.25° reveal its cubic lattice structure assigned to the planes.

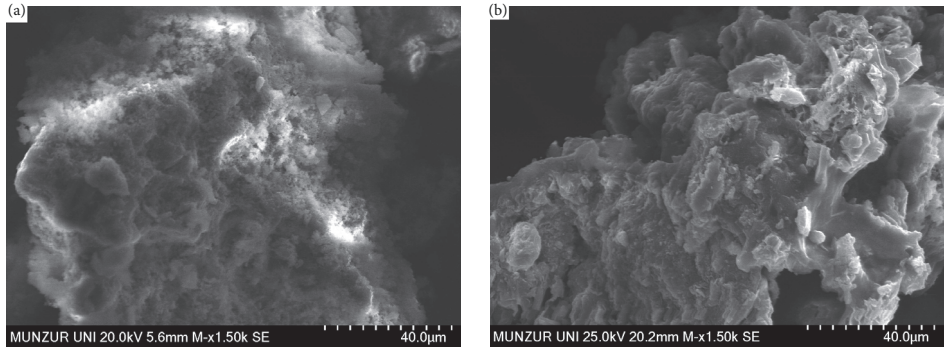

(a) (b)

Figure 2: SEM pictures of the poly(AN-co-VP)/zeolite composite (a) before adsorption and (b) after adsorption.

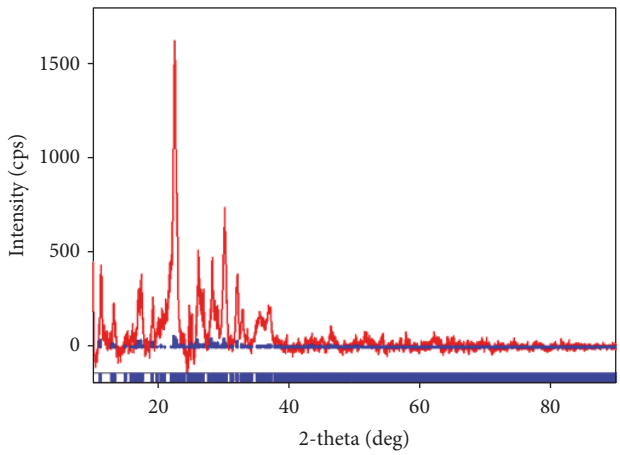

Figure 3: XRD analysis of the poly(AN-co-VP)/zeolite composite.

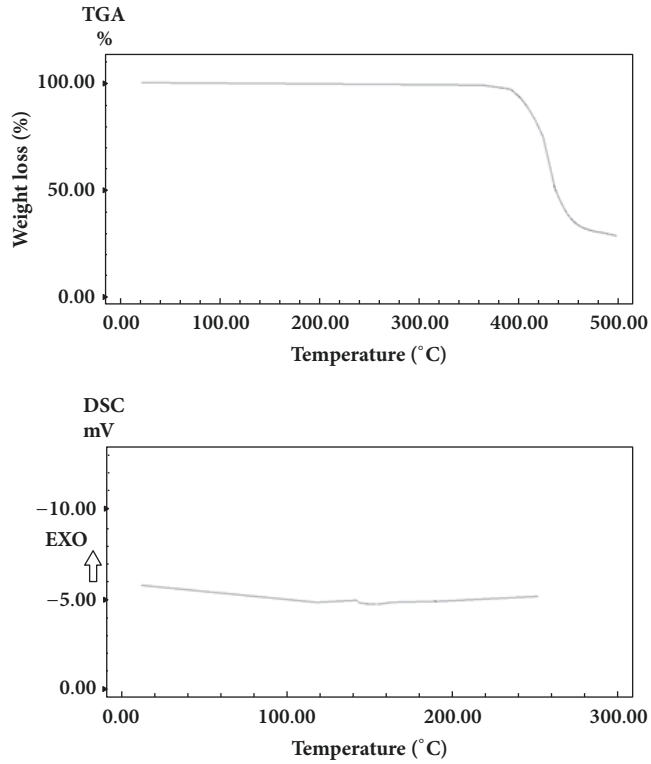

Figure 4: (a) TGA and (b) DSC curves of the poly(AN-co-VP)/zeolite composite.

To investigate the thermal stability of the composite, TGA and DSC measurements were taken under the nitrogen atmosphere and the results are shown in Figure 4. According to Figure 4(a), the decomposition temperature is 410°C and the decomposition occurs in a single stage. This value indicates that the composite is quite stable. Also, residue of the composite at 500°C is around 25%. It is thought that the amount of this waste is derived from the zeolite. In DSC curve (Figure 4(b)), it can clearly be seen that the glass transition temperature (T_g) of the composite is 152°C.

3.2. Adsorption Studies

3.2.1. Adsorption Isotherms. The adsorption isotherms explain the relationship between the adsorbent and adsorbate and give an idea about the adsorption capacity at a certain temperature. They are important in terms of providing information about the surface properties and explaining the mechanism of adsorption. Furthermore, they play an important role in setting up the necessary physicochemical conditions for better understanding and designing the adsorption process. Apart from the available various isotherm models used to investigate adsorption equilibrium in the literature, two models, namely, the Langmuir and Freundlich isotherm models, are most commonly used to describe equilibrium adsorption [35, 36]. The Langmuir model successfully explains that the adsorption process takes place in a monolayer on a homogeneous surface. The linear Langmuir equation is expressed by the following relation [37]:

$$\frac{C_e}{q_e} = \frac{1}{K_L} + \frac{a_L}{K_L} C_e \quad (4)$$

where q_e (mg/g) and C_e (mg/L) are the amounts of adsorbed dye and unadsorbed dye concentrations in a solution at

Table 2: Isotherm coefficients for BG adsorbed onto the poly(VP-co-An)/zeolite.

	Langmuir model			Freundlich model		
T, °C	q_{max}	a_L	R^2	K_F	n	R^2
20	16.95	0.413	0.992	5.737	3.030	0.978
30	19.61	0.490	0.989	6.547	2.632	0.989
40	23.81	0.575	0.999	8.331	2.457	0.949

Table 3: Comparison of maximum adsorbent capacity of BG with different sorbents.

Adsorbent	Maximum adsorbent capacity (q_{max})	References
'Saklıkent' mud	1.18	[27]
Modified chitosan	10.91	[28]
Luffa cylindrical sponge	18.52	[29]
Rice husk ash	26	[30]
Tannin gel	8.55	[31]
$MnFe_2O_4$	0. 82	[32]
$CuFe_2O_4$	0.775	[32]
$Mn_{0.5}Cu_{0.5}Fe_2O_4$	0.86	[32]
Poly(AN-co-VP)/zeolite composite	23.81	This study

equilibrium, respectively. K_L (L/g) is the adsorption isotherm constant and a_L (L/mg) is the monolayer adsorption capacity related to the energy. The maximum adsorption capacity of the adsorbent (q_{max}) is numerically calculated from K_L/a_L.

The Freundlich model is an exponential equation that exhibits adsorption on heterogeneous surfaces and it is also used for examining adsorption equilibrium in non-monolayer surfaces. The linear Freundlich equation is expressed by the following equation [38]:

$$\ln q_e = \ln K_F + \frac{1}{n} \ln C_e \tag{5}$$

where C_e (mg/L) is equilibrium concentration, K_F (mg/g) is the Freundlich constants related to the amount of dye adsorbed on the adsorbent, and n is the applicability of adsorbent. The value of n between 1 and 10 shows suitable adsorption process. K_F and n were calculated from the slope and the intercept of the linear plot, respectively.

The constants and the correlation coefficient (R^2) values calculated for the two equilibrium models are given in Table 2. The data were investigated for three different temperatures and compared. It was seen that the value of R^2 for Langmuir isotherm was higher than the value obtained for the Freundlich isotherm. A higher value of R^2 demonstrated that the adsorption isotherm for BG onto the poly(AN-co-VP)/zeolite composite is explained better by the Langmuir model [39]. The maximum adsorption capacity was obtained as 23.81 mg/g from Langmuir isotherm. This capacity was compared with many reported adsorbents and they are shown in Table 3. Furthermore, the value n was above 1 (3.030, 2.632, 2.457), indicating that BG was favorably adsorbed onto the composite.

3.2.2. Adsorption Kinetics. The kinetics of the dye removal process were studied by using pseudo-first-order, pseudo-second-order, intraparticle diffusion, and external mass transfer kinetic models. Pseudo-first and pseudo-second-order kinetic studies were performed at different temperatures (20-40°C), constant composite dose (0.2 g/50 mL), and constant dye concentration (50 mg/L). Intraparticle diffusion and external mass transfer kinetic models were performed at different dye concentrations (25-100 mg/L), different temperatures (20-40°C), and constant composite dose (0.2 g/50 mL). The equations for the pseudo-first-order, pseudo-second-order, intraparticle diffusion, and external mass transfer kinetic models are as follows, respectively [40]:

$$\ln (q_e - q_t) = \ln q_e - k_1 t \tag{6}$$

$$\frac{t}{q_t} = \frac{1}{k_2 q_e^2} + \left(\frac{1}{q_e}\right) t \tag{7}$$

$$q_t = k_i t^{1/2} \tag{8}$$

$$\frac{d\,(C/C_0)}{dt} = -k_L S \tag{9}$$

where q_e and q_t (mg/g) are the adsorption capacities of BG at equilibrium and at time t, respectively. k_1 (1/min) is the pseudo-first-order rate constant, k_2 (1/min) is the pseudo-second-order rate constant, k_i (mg/gmin$^{1/2}$) is the intraparticle diffusion rate constant, C is the BG concentration in t time (mg/L), C_o is the initial BG concentration (mg/L), and S is the specific surface area for mass transfer. The change of pseudo-first- and pseudo-second-order rate constants with temperature and the exchange of intraparticle diffusion rate constants and external mass transfer coefficients with temperature and different initial BG concentration are summarized in Tables 4 and 5, respectively.

In pseudo-first-order, plot $\ln(q_e - q_t)$ versus t gives a straight line and the values of k_1 and q_e were determined using this straight line. For pseudo-second-order, the graph of t/q_t versus t was used to calculate q_e and k_2 from slope and intercept, respectively. It is clear in Table 4 that the calculated q_e ($q_{e,cal}$) value found from the graph is much lower than the experimental q_e ($q_{eq,exp}$) value and low regression coefficient of BG. This demonstrates that pseudo-first-order cannot be applied for this adsorption experiment. Higher values of regression coefficient for pseudo-second-order illustrate greater harmony of BG adsorption than pseudo-first-order for all temperatures. Also in this kinetic model the $q_{eq,cal}$ and the $q_{eq,exp}$ values were very close to each other. For these reasons, pseudo-second-order model is better complied with the data [41, 42].

Table 4: The change with temperature on pseudo-first- and pseudo-second-order reaction rate constants.

T	$q_{eq,exp}$	Pseudo-first-order kinetic model			Pseudo-second-order kinetic model		
		k_1	$q_{eq,cal}$	R^2	k_2	$q_{eq,cal}$	R^2
°C	mg/g	1/min	mg/g		1/min	mg/g	
20	11.11	0.04375	7.35	0.956	0.01170	11.63	0.999
30	11.58	0.04836	3.50	0.806	0.04722	11.76	0.999
40	12.03	0.05296	2.32	0.925	0.12019	12.20	0.999

Table 5: Exchange with initial BG concentration and temperature on the intraparticle diffusion rate constants (k_i) and external mass transfer coefficients (k_L).

C_o	20°C		30°C		40°C	
	ki	k_L	ki	k_L	ki	k_L
mg/L	mg/g min$^{1/2}$	cm/min	mg/g min$^{1/2}$	cm/min	mg/g min$^{1/2}$	cm/min
25	0.404	0.020075	0.467	0.045994	0.518	0.051407
50	1.022	0.019750	1.108	0.043288	1.452	0.045994
75	1.536	0.018938	1.826	0.032469	2.121	0.040588
100	1.745	0.015694	2.125	0.027057	2.753	0.035175

The external mass transfer model is related to the liquid-solid external mass transfer coefficient k_L (cm/min) in the change of dye concentration over time. For the studied external mass transfer of BG onto the poly(VP-co-An)/zeolite, the plot $\ln(q_e - q_t)$ versus t gives a straight line and the k_L values were determined from the slope in all initial dye concentrations (25-100 mg/L) and at all temperatures (20, 30, 40°C). Findings showed that external mass transfer coefficients decreased with increasing initial BG concentration while they increased with increasing temperature. This increase in the coefficients can be attributed to the increase of kinetic energy and mobility of the BG molecules as the temperature increases. The external mass transfer is not negligible although this effect is important at the beginning of the adsorption [40].

q_t curves against the $t^{1/2}$ found at 20, 30, and 40°C and in all initial dye concentrations (25, 50, 75, 100 mg/L) consist of three steps. The first part is a sharply increasing section, and the second linear part shows the rate-limiting step of intraparticle diffusion. The third part is a slower internal diffusion part than other steps due to the decrease in the dye concentration in solution. For each concentration and temperature, k_i values were calculated from these linear parts and displayed in Table 5. In the table, it is clear that k_i values increased with increasing temperature and initial BG concentrations. For each temperature and concentration, linear curves of the second part did not pass through the origin. This demonstrates that the border layer control had some steps, and it also indicates that intraparticle diffusion was not the step solely controlling the rate [40].

An adsorption mechanism as shown in Figure 5 may be proposed for the adsorption of BG onto the composite, taking into account the chemical properties of the adsorbate and the adsorbent. The high adsorption capacity can be due to π-π interactions between the dye molecules containing aromatic ring and the poly(VP-co-An)/zeolite composite [43]. Meanwhile, van der Waals interactions have a significant effect on the amount of this adsorption.

Table 6: Thermodynamic parameters for BG adsorption.

T, °C	ΔH^o, kJ/mol	ΔG^o, kJ/mol	ΔS^o, kJ/molK
20	12.67	-29.72	0.14
30		-31.17	
40		-32.62	

3.2.3. Adsorption Thermodynamics. The thermodynamic parameters such as a changes in Gibbs-free energy (ΔG^o), enthalpy (ΔH^o), and entropy (ΔS^o) for BG adsorption onto the poly(VP-co-An)/zeolite composite were calculated from the equations given below:

$$\Delta G^o = -RT \ln K_C \quad (10)$$

$$\Delta G^O = \Delta H^o - T\Delta S^o \quad (11)$$

$$\ln K_C = \frac{\Delta S^o}{R} - \frac{\Delta H^o}{RT} \quad (12)$$

where R (8.314 J/mol K) is the universal gas constant, T (K) is the absolute temperature, and K_C is the equilibrium constant and it was calculated by using Langmuir constant (a_L) and molecular weight of BG (482.64 g/mol) [44]. Here, ΔH^o and ΔS^o were calculated from the slope and intercept of the graph of the ln b versus 1/T.

The adsorption of solid materials is divided into physical and chemical adsorption. When compared to chemical adsorption the energy change for physical adsorption is lower than 40 kJ/mol while chemical adsorption changes from 40 kJ/mol to 120 kJ/mol [33]. As seen from Table 6 the adsorption process is physical according to the ΔH^o value. The negative value of ΔG^o shows that adsorption takes place spontaneously and exothermically at three different temperatures (20, 30, 40°C). Furthermore, the positive value of ΔS^o indicates that the solid-liquid interface is random during adsorption [45]. As a result, the adsorption of BG onto the poly(VP-co-An)/zeolite composite is more favorable.

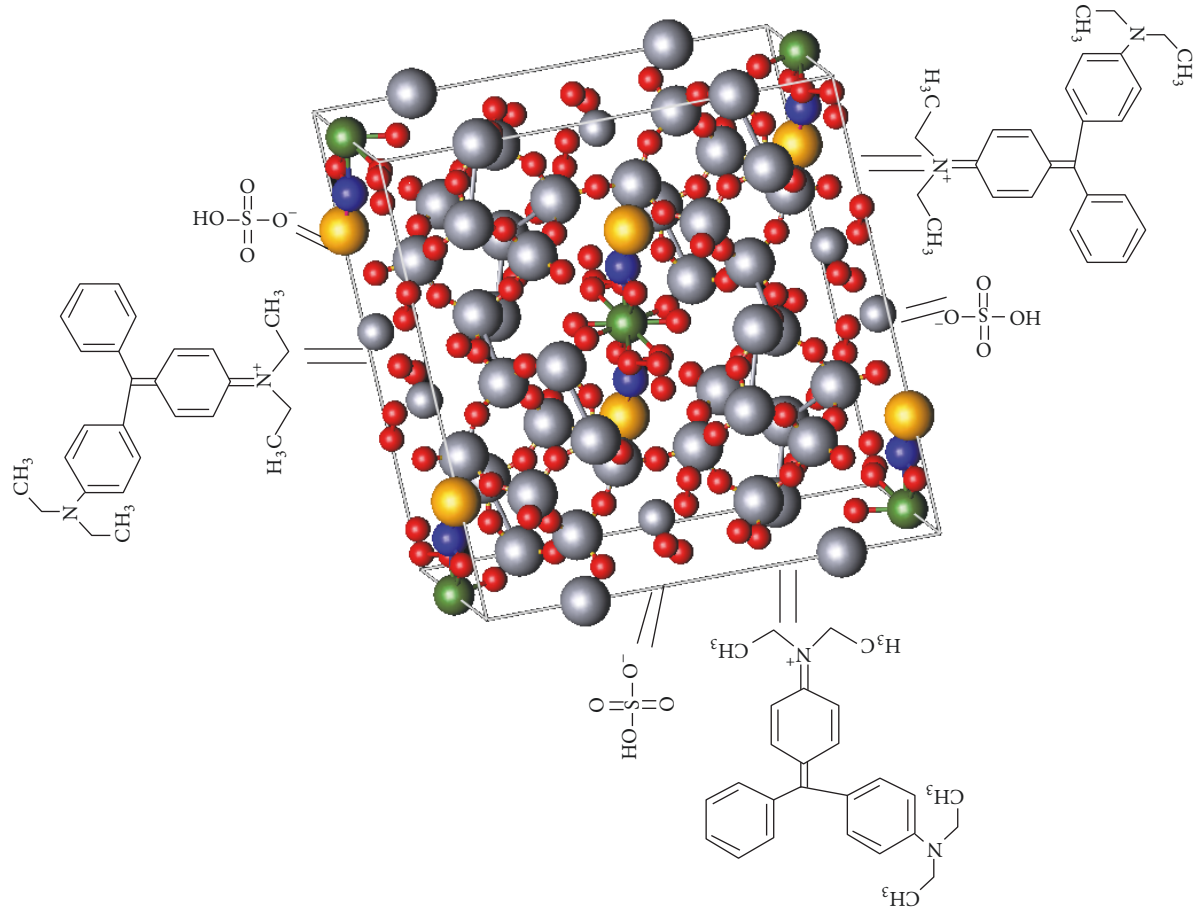

Figure 5: Schematic illustration of the adsorption process and interactions between the composite and BG.

3.3. CCD Optimization

3.3.1. ANOVA for Response Surface Quadratic Model. The experimental design including coded values of selected parameters and the observed and actual responses is shown in Table 7. Equation (13) indicates quadratic relationship between the response and independent parameters for the BG.

$$\begin{aligned}\text{BG Removal } (\%) = {} & +80.92 + 12.34A - 7.94B \\ & + 4.47C + 2.98AB - 0.82AC \\ & + 1.96B - 4.11A^2 + 1.76B^2 \\ & + 2.45C^2\end{aligned} \tag{13}$$

In (13), negative signs indicate antagonistic effect, whereas positive signs show the synergistic effect. As seen from (13), A (adsorbent mass) and B (time) are both positive. This shows that BG adsorption onto poly(VP-co-An)/zeolite will increase when these parameters are increased [46]. The significance of each term was established by p-value (Prob>F), which is shown in Table 8. According to this table, the model terms A, B, C, and A^2 were significant, with a p-value being less than 0.05. The other model terms were insignificant (p> 0.05).

As shown in Table 8 (ANOVA), the model fit of the data is more significant. F-value (21.30) and p-value (<0.0001) of the model imply that it is quite important for BG adsorption onto poly(VP-co-AN)/zeolite. The high value of correlation coefficient (R^2 = 0.95) indicated that only 5% of the total variation could not be described by the model. The higher value of R^2 demonstrated the better fitness of the regression model in the studied experimental set [47]. Furthermore, the value of adjusted R^2 (0.91) confirmed that the BG removal of the model is a significant parameter indicating good harmony between the experimental and predicted removal yield. Hence, the applied model is enough to make predictions at the interval of experimental factors. The adequate precision measures the signal to noise ratio. The ratio is required to be higher than 4 for a well model [46]. In this work, the adequate precision ratio of the model was found to be 16.487, which implied that there was an adequate signal. The coefficient of variation (CV) defines reliability of the model and is the ratio of the standard deviation as a percentage of the mean value of the observed response [48]. If CV of the model is lower than 10%, the model can be considered reproducible, and in the present study, the CV value was 5.45.

3.3.2. Response Surfaces and Contour Plots for BG Adsorption. The 3-dimensional response surface (3D) and 2-dimensional contour plots (2D) (Figure 6) were plotted based on the

Table 7: Experimental parameters and levels in the CCD for the BG removal.

Factors	Units	Levels				
		- α(1.68)	Low (-1)	Central (0)	High (+1)	+α(1.68)
A: Adsorbent mass	g/50 mL	0.05	0.091	0.15	0.21	0.25
B: BG concentration	mg/L	25	40.20	62.50	84.80	100
C: Time	min	10	38.38	80	121.62	150
	Factors			Response (BG removal, %)		
Run	*A*	*B*	*C*	Observed	Predicted	Residual
1	1.682	0	0	91.94	90.04	1.90
2	-1	-1	-1	80.21	76.26	3.95
3	1	-1	1	99.68	100.00	-0.32
4	0	0	0	80.91	80.92	-0.01
5	-1	1	1	71.30	65.02	6.28
6	0	0	-1.682	77.16	80.33	-3.17
7	0	0	0	80.91	80.92	-0.01
8	-1.682	0	0	41.31	48.54	-7.23
9	0	0	0	80.72	80.92	-0.20
10	1	1	1	93.83	94.01	-0.18
11	0	0	0	82.07	80.92	1.15
12	1	-1	-1	94.12	96.63	-2.51
13	0	0	0	80.91	80.92	-0.01
14	0	0	1.682	93.21	95.37	-2.16
15	-1	1	-1	54.61	50.52	4.09
16	-1	-1	1	83.84	82.93	0.91
17	0	-1.682	0	99.87	99.25	0.62
18	0	1.682	0	66.62	72.56	-5.94
19	0	0	0	80.91	80.92	-0.01
20	1	1	-1	85.66	82.80	2.86

Table 8: ANOVA for BG removal.

Source	Sum of squares	Df[a]	Mean square	*F*- Value	*P*-value Prob > F	Status
Model	3734.695	9	414.9661	21.29753	< 0.0001	significant
A	2078.46	1	2078.46	106.674	< 0.0001	
B	859.93	1.00	859.93	44.13	< 0.0001	
C	272.85	1.00	272.85	14.00	0.0038	
AB	70.98	1.00	70.98	3.64	0.0854	
AC	5.43	1.00	5.43	0.28	0.6091	
BC	30.69	1.00	30.69	1.58	0.2380	
A^2	243.64	1.00	243.64	12.50	0.0054	
B^2	44.86	1.00	44.86	2.30	0.1601	
C^2	86.52	1.00	86.52	4.44	0.0613	
Residual	194.84	10.00	19.48			
Lack-of-fit	193.62	5.00	38.72	158.07		
Pure error	1.22	5.00	0.24			
Cor total	3929.54	19.00				
R^2			0.95			
R^2-Adjusted			0.91			
R^2-Predicted			0.62			
CV%[b]			5.45			
Adequate precision			16.487			

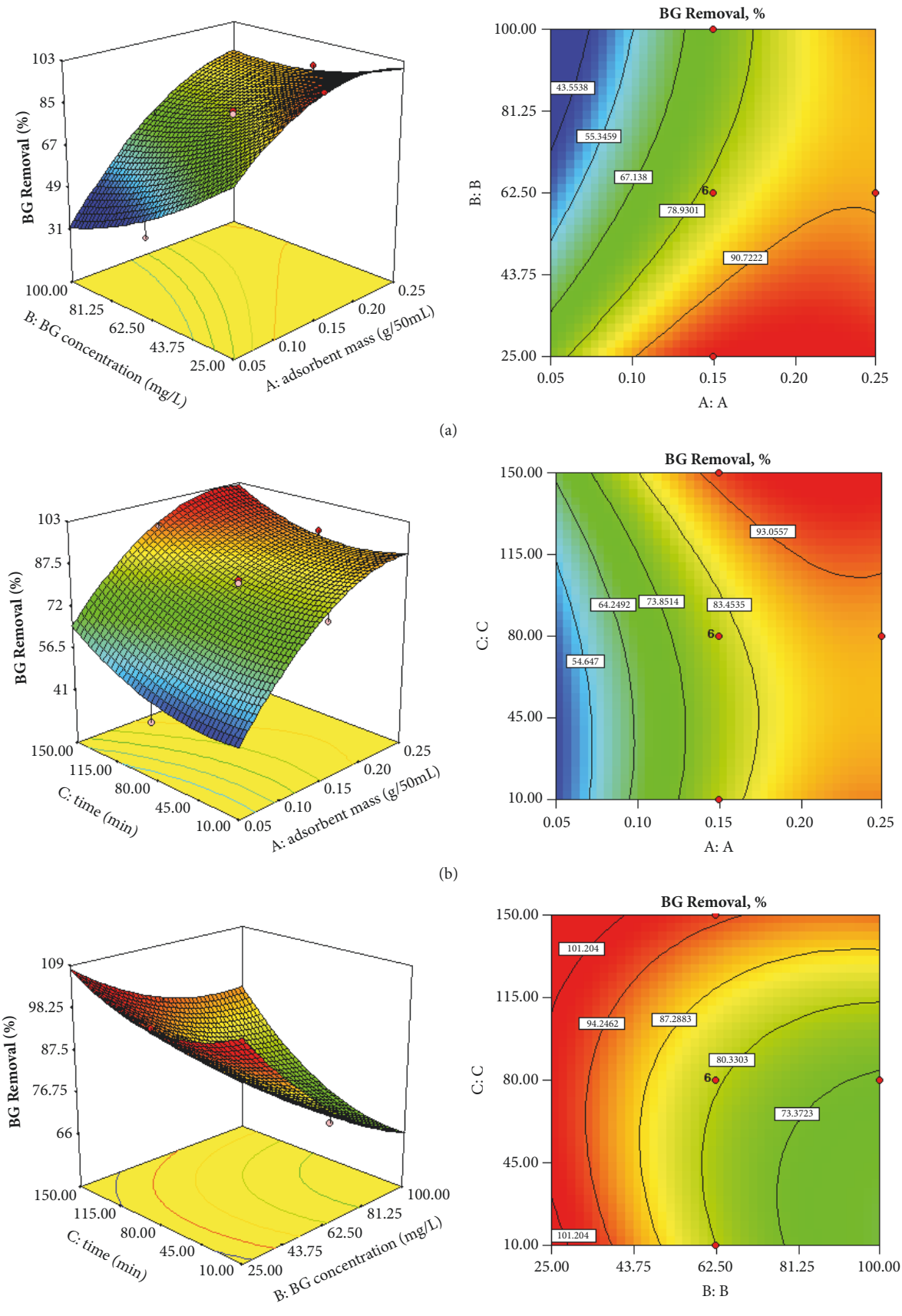

Figure 6: 3D response surface and 2D contour plots of combined effects of (a) *AB*, (b) *AC*, and (c) *BC* on the BG removal by onto poly(VP-co-An)/zeolite.

quadratic model in order to investigate the interactive effect of the tested parameters on the removal of BG. The response surface plots and corresponding contour plots were utilized to understand the interaction and individual effects of the chosen independent factors [49]. Response surface plots can be taken into account as an approach to estimating the removal yield (%) for different values of the studied parameters. Furthermore, 2D contour plots are beneficial to determine the type of interactions between the tested factors. Figure 6(a) illustrates the response surface and contour plots as a function of the initial BG concentration and adsorbent mass while the time was kept constant at 80 min. As shown, with the increasing of the initial BG concentration, the removal yield of dye was decreased. The decrease in dye removal percentage at high BG concentrations could be due to the saturation of dye-binding sites of the adsorbent. Increasing adsorbent mass ensured more surface area, thereby leading to more binding regions for the adsorption of dye onto poly(VP-co-An)/zeolite [50]. Figure 6(b) shows the interaction effect of the adsorbent mass and the time on the dye removal yield when the initial BG concentration was constant at 62.50 mg/L. It was observed that the BG removal efficiency increased with enhancing in adsorbent mass. It can be concluded that the availability of active sites increased with increasing the adsorbent mass [51, 52]. Figure 6(c) shows the effects of initial BG concentration and time on the removal yield of BG while the adsorbent mass was kept constant at 0.15 mg/50 mL. It was observed that at lower BG concentrations, the ratio of solute concentrations to free reactive adsorbent sites is lower and speeds dye removal which leads to an increment in dye adsorption, and at higher concentrations due to the saturation of adsorption areas the removal yield was reduced [52, 53].

The effect of selected adsorption parameters was optimized to reach optimal removal yield based on using the desirability function at the CCD [54, 55]. According to this desirability function, the optimum values were found to be an adsorbent mass of 0.20 g/50 mL, an initial BG concentration of 40.20 mg/L, and a time of 121.60 min, which will result in 99.91% removal of BG with 0.1000 desirability.

4. Conclusion

This study showed that the poly(VP-co-An)/zeolite composite prepared by FRP is an effective adsorbent for the removal of BG from aqueous solutions. A CCD was applied to determine the interactions among factors; the optimum values of three significant parameters, namely, time, adsorbent mass, and initial BG concentration, showed significant effect on adsorption process. The optimum values were found to be an adsorbent mass of 0.20 g/50 mL, an initial BG concentration of 40.20 mg/L, and a time of 121.60 min for maximum BG removal. A second-order quadratic model was developed to describe the behavior of adsorption process using Design Expert software. This mathematical model was used to develop contour plots for three factors effects. The significance of independent factors was tested by analysis of variance (ANOVA). According to ANOVA results, all of the variables have the linear effect on BG adsorption process. Both external mass transfer and internal particle diffusion played an important role in the adsorption kinetics of BG, and the adsorption process followed a pseudo-second-order kinetic model which has a higher correlation coefficient. Furthermore, the equilibrium isotherm was better explained by the Langmuir model. According to the results, this composite is of great importance since it has a higher maximum adsorption capacity than many of the adsorbents reported in the literature.

Data Availability

No data were used to support this study.

Conflicts of Interest

The authors declare that they have no conflicts of interest.

References

[1] M. H. Dehghania, A. Dehghana, and A. Najafpoor, "Removing Reactive Red 120 and 196 using chitosan/zeolite composite from aqueous solutions: Kinetics, isotherms, and process optimization," *Journal of Industrial and Engineering Chemistry*, vol. 51, pp. 185–195, 2017.

[2] N. F. Cardoso, E. C. Lima, B. Royer et al., "Comparison of Spirulina platensis microalgae and commercial activated carbon as adsorbents for the removal of Reactive Red 120 dye from aqueous effluents," *Journal of Hazardous Materials*, vol. 241-242, pp. 146–153, 2012.

[3] A. Çelekli, F. Çelekli, E. Çiçek, and H. Bozkurt, "Predictive modeling of sorption and desorption of a reactive azo dye by pumpkin husk," *Environmental Science and Pollution Research*, vol. 21, no. 7, pp. 5086–5097, 2014.

[4] B. K. Nandi, A. Goswami, and M. K. Purkait, "Adsorption characteristics of brilliant green dye on kaolin," *Journal of Hazardous Materials*, vol. 16, pp. 387–395, 2009.

[5] Y. Kismir and A. Z. Aroguz, "Adsorption characteristics of the hazardous dye Brilliant Green on Saklıkent mud," *Chemical Engineering Journal*, vol. 172, no. 1, pp. 199–206, 2011.

[6] M. K. Dahri, L. B. L. Lim, M. R. R. Kooh, and C. M. Chan, "Adsorption of brilliant green from aqueous solution by unmodified and chemically modified Tarap (Artocarpus odoratissimus) peel," *International Journal of Environmental Science and Technology*, vol. 14, no. 12, pp. 2683–2694, 2017.

[7] K. G. Bhattacharyya and A. Sarma, "Adsorption characteristics of the dye, Brilliant Green, on Neem leaf powder," *Dyes and Pigments*, vol. 57, no. 3, pp. 211–222, 2003.

[8] V. K. Gupta and Suhas, "Application of low-cost adsorbents for dye removal–a review," *Journal of Environmental Management*, vol. 90, no. 8, pp. 2313–2342, 2009.

[9] S. Salahi and M. Ghorbani, "Adsorption parameters studies for the removal of mercury from aqueous solutions using hybrid sorbent," *Advances in Polymer Technology*, vol. 33, no. 4, p. 1, 2014.

[10] G. Crini, "Non-conventional low-cost adsorbents for dye removal: a review," *Bioresource Technology*, vol. 97, no. 9, pp. 1061–1085, 2006.

[11] M. Arulkumar, P. Sathishkumar, and T. Palvannan, "Optimization of Orange G dye adsorption by activated carbon of

Thespesia populnea pods using response surface methodology," *Journal of Hazardous Materials*, vol. 186, no. 1, pp. 827–834, 2011.

[12] M. Bin and W. Aiqin, "Adsorption of dyes onto palygorskite and its composites: a review," *Journal of Environmental Chemical Engineering*, vol. 4, no. 1, pp. 1274–1294, 2016.

[13] R. C. Bansal and M. Goyal, *Activated Carbon Adsorption*, Taylor and Francis Group, Boca Raton, Fla, USA, 1st edition, 2005.

[14] T. Senthilkumar, R. Raghuraman, and L. R. Miranda, "Parameter optimization of activated carbon production from Agave sisalana and Punica granatum peel: adsorbents for C.I. reactive orange 4 removal from aqueous solution," *Clean-Soil, Air, Water*, vol. 41, pp. 797–807, 2013.

[15] W. S. Wan Ngah, N. F. M. Ariff, and M. A. K. M. Hanafiah, "Preparation, characterization, and environmental application of crosslinked chitosan-coated bentonite for tartrazine adsorption from aqueous solutions," *Water, Air, & Soil Pollution*, vol. 206, no. 1-4, pp. 225–236, 2010.

[16] V. Nguyen, W. Yoshida, J. D. Jou, and Y. Cohen, "Kinetics of free-radical graft polymerization of 1-vinyl-2-pyrrolidone onto silica," *Journal of Polymer Science Part A: Polymer Chemistry*, vol. 40, pp. 26–42, 2002.

[17] J. G. Hefferman and D. C. Sherrington, "Polystyrene gel permeation chromatography packings grafted with polar monomers—synthesis and use in aqueous organic mobile phases," *Journal of Applied Polymer Science*, vol. 29, pp. 3013–3025, 1984.

[18] S. Janakiraman, S. L. Farrell, C.-Y. Hsieh, Y. Y. Smolin, M. Soroush, and K. K. S. Lau, "Kinetic analysis of the initiated chemical vapor deposition of poly(vinylpyrrolidone) and poly(4-vinylpyridine)," *Thin Solid Films*, vol. 595, pp. 244–250, 2015.

[19] S. Staufenbiel, M. Merino, W. Li, S. Huang, A. Lendlein, R. H. Müller et al., "Surface characterization and protein interaction of a series of model poly[acrylonitrile-co-(N-vinyl pyrrolidone)] nanocarriers for drug targeting," *International Journal of Pharmaceutics*, vol. 485, no. 1-2, pp. 87–96, 2015.

[20] L. Wan, Z. Xu, X. Huang, Z. Wang, and P. Ye, "Hemocompatibility of Poly(acrylonitrile-co-N-vinyl-2-pyrrolidone)s: swelling behavior and water states," *Macromolecular Bioscience*, vol. 5, no. 3, pp. 229–236, 2005.

[21] N. Zhang, A. Said, C. Wischke et al., "Poly[acrylonitrile-co-(N-vinyl pyrrolidone)] nanoparticles – Composition-dependent skin penetration enhancement of a dye probe and biocompatibility," *European Journal of Pharmaceutics and Biopharmaceutics*, vol. 116, pp. 66–75, 2017.

[22] M. A. Salem, R. G. Elsharkawy, and M. F. Hablas, "Adsorption of brilliant green dye by polyaniline/silver nanocomposite: Kinetic, equilibrium, and thermodynamic studies," *European Polymer Journal*, vol. 75, pp. 577–590, 2016.

[23] M. Ghaedi, A. Ansari, F. Bahari, A. M. Ghaedi, and A. Vafaei, "A hybrid artificial neural network and particle swarm optimization for prediction of removal of hazardous dye brilliant green from aqueous solution using zinc sulfide nanoparticle loaded on activated carbon," *Spectrochimica Acta, Part A: Molecular and Biomolecular Spectroscopy*, vol. 137, pp. 1004–1015, 2015.

[24] V. Srivastava, Y. C. Sharma, and M. Sillanpää, "Application of response surface methodology for optimization of Co(II) removal from synthetic wastewater by adsorption on NiO nanoparticles," *Journal of Molecular Liquids*, vol. 211, pp. 613–620, 2015.

[25] N. Chaudhary and C. Balomajumder, "Optimization study of adsorption parameters for removal of phenol on aluminum impregnated fly ash using response surface methodology," *Journal of the Taiwan Institute of Chemical Engineers*, vol. 45, no. 3, pp. 852–859, 2014.

[26] P. F. Sales, Z. M. Magriotis, M. A. L. S. Rossi, R. F. Resende, and C. A. Nunes, "Optimization by Response Surface Methodology of the adsorption of Coomassie Blue dye on natural and acid-treated clays," *Journal of Environmental Management*, vol. 130, pp. 417–428, 2013.

[27] Y. Kismir and A. Z. Aroguz, "Adsorption characteristics of the hazardous dye brilliant green on saklikent mud," *Chemical Engineering Journal*, vol. 172, pp. 199–206, 2011.

[28] H. Karaer and I. Uzun, "Adsorption of basic dyestuffs from aqueous solution by modified chitosan," *Desalination and Water Treatment*, vol. 51, pp. 2294–2305, 2013.

[29] O. S. Esan, O. N. Abiola, O. Owoyomi, C. O. Aboluwoye, and M. O. Osundiya, "Adsorption of brilliant green onto luffa cylindrical sponge: equilibrium, kinetics, and thermodynamic studies," *ISRN Physical Chemistry*, vol. 2014, Article ID 743532, 12 pages, 2014.

[30] V. S. Mane, I. DeoMall, and V. Chandra Srivastava, "Kinetic and equilibrium isotherm studies for the adsorptive removal of Brilliant Green dye from aqueous solution by rice husk ash," *Journal of Environmental Management*, vol. 84, pp. 390–400, 2007.

[31] N. Akter, A. Hossain, M. J. Hassan et al., "Amine modified tannin gel for adsorptive removal of Brilliant Green dye," *Journal of Environmental Chemical Engineering*, vol. 4, no. 1, pp. 1231–1241, 2016.

[32] S. Hashemian, A. Dehghanpor, and M. Moghahed, "Cu0.5Mn0.5Fe2O4 nano spinels as potential sorbent for adsorption of brilliant green," *Journal of Industrial and Engineering Chemistry*, vol. 24, pp. 308–314, 2015.

[33] G. Torgut, M. Tanyol, F. Biryan, G. Pihtili, and K. Demirelli, "Application of response surface methodology for optimization of remazol brilliant blue R removal onto a novel polymeric adsorbent," *Journal of the Taiwan Institute of Chemical Engineers*, vol. 80, pp. 406–414, 2017.

[34] A. Vanamudan, K. Bandwala, and P. Pamidimukkala, "Adsorption property of Rhodamine 6G onto chitosan-g-(N-vinyl pyrrolidone)/montmorillonite composite," *International Journal of Biological Macromolecules*, vol. 69, pp. 506–513, 2014.

[35] X. Jiang, D. Zhou, X. Huang, W. Zhao, and C. Zhao, "Hexanediamine functionalized poly (glycidyl methacrylate-co-N-vinylpyrrolidone) particles for bilirubin removal," *Journal of Colloid and Interface Scienc*, vol. 504, pp. 214–222, 2017.

[36] D. Cao, X. Yang, G. Geng et al., "Absorption and subcellular distribution of cadmium in tea plant (Camellia sinensis cv. "Shuchazao")," *Environmental Science and Pollution Research*, vol. 25, pp. 15357–15367, 2018.

[37] G. Crini and P. M. Badot, "Application of chitosan, a natural aminopolysaccharide, for dye removal from aqueous solutions by adsorption processes using batch studies: a review of recent literature," *Progress in Polymer Science*, vol. 33, pp. 399–447, 2008.

[38] M. Fayazi, M. Ghanei-Motlagh, and M. A. Taher, "The adsorption of basic dye (Alizarin red S) from aqueous solution onto activated carbon/γ-Fe2O3 nano-composite: kinetic and equilibrium studies," *Materials Science in Semiconductor Processing*, vol. 40, pp. 35–43, 2015.

[39] D. Wang, L. Liu, X. Jiang, J. Yu, and X. Chen, "Adsorption and removal of malachite green from aqueous solution using

magnetic beta-clodextrin-graphene oxide nanocomposites as adsorbents," *Colloids and Surfaces A–Physicochemical and Engineering Aspects*, vol. 466, pp. 166–173, 2015.

[40] M. Tanyol, V. Yonten, and V. Demir, "Removal of phosphate from aqueous solutions by chemical- and thermal-modified bentonite clay," *Water, Air, and Soil Pollution*, vol. 226, no. 8, 2015.

[41] M. T. Yagub, T. K. Sen, S. Afroze, and H. M. Ang, "Dye and its removal from aqueous solution by adsorption: a review," *Advances in Colloid and Interface Science*, vol. 209, pp. 172–184, 2014.

[42] N. Kataria and V. K. Garg, "Removal of Congo red and Brilliant green dye from aqueous solution using flower shaped ZnO nanoparticles," *Journal of Environmental Chemical Engineering*, vol. 5, no. 6, pp. 5420–5428, 2017.

[43] B. Yan, Z. Chen, L. Cai, J. Fu, and Q. Xu, "Fabrication of polyaniline hydrogel: synthesis, characterization and adsorption of methylene blue," *Applied Surface Science*, vol. 356, pp. 39–47, 2015.

[44] J. Lin, S. He, X. Wang, H. Zhang, and Y. Zhan, "Removal of phosphate from aqueous solution by a novel $Mg(OH)_2/ZrO_2$ composite: adsorption behavior and mechanism," *Colloids and Surfaces A: Physicochemical and Engineering Aspects*, vol. 561, pp. 301–314, 2019.

[45] W. Liu, C. Yao, M. Wang, J. Ji, L. Ying, and C. Fu, "Kinetics and thermodynamics characteristics of cationic yellow X-GL adsorption on attapulgite/rice hull-based activated carbon nanocomposites," *Environmental Progress and Sustainable Energy*, vol. 32, pp. 655–662, 2013.

[46] H. Radnia, A. R. Solaimany Nazar, and A. Rashidi, "Experimental assessment of graphene oxide adsorption onto sandstone reservoir rocks through response surface methodology," *Journal of the Taiwan Institute of Chemical Engineers*, vol. 80, pp. 34–45, 2017.

[47] M. Dastkhoon, M. Ghaedi, A. Asfaram, A. Goudarzi, S. M. Mohammadi, and S. Wang, "Improved adsorption performance of nanostructured composite by ultrasonic wave: Optimization through response surface methodology, isotherm and kinetic studies," *Ultrasonics Sonochemistry*, vol. 37, pp. 94–105, 2017.

[48] E. A. Dil, M. Ghaedi, A. Ghaedi et al., "Modeling of quaternary dyes adsorption onto ZnO–NR–AC artificial neural network: Analysis by derivative spectrophotometry," *Journal of Industrial and Engineering Chemistry*, vol. 34, pp. 186–197, 2016.

[49] A. Hassani, A. Khataee, S. Karaca, M. Karaca, M. Kiransan, and M. Kıranşan, "Adsorption of two cationic textile dyes from water with modified nanoclay: a comparative study by using central composite design," *Journal of Environmental Chemical Engineering*, vol. 3, no. 4, pp. 2738–2749, 2015.

[50] E. A. Dil, M. Ghaedi, and A. Asfaram, "The performance of nanorods material as adsorbent for removal of azo dyes and heavy metal ions: application of ultrasound wave, optimization and modeling," *Ultrasonics Sonochemistry*, vol. 34, pp. 792–802, 2017.

[51] F. Khodam, Z. Rezvani, and A. R. Amani-Ghadim, "Enhanced adsorption of acid red 14 by co-assembled LDH/MWCNTs nanohybrid: optimization, kinetic and isotherm," *Journal of Industrial and Engineering Chemistry*, vol. 21, pp. 1286–1294, 2015.

[52] M. H. A. Azqhandi, M. Ghaedi, F. Yousefi, and M. Jamshidi, "Application of random forest, radial basis function neural networks and central composite design for modeling and/or optimization of the ultrasonic assisted adsorption of brilliant green on ZnS-NP-AC," *Journal of Colloid and Interface Science*, vol. 505, pp. 278–292, 2017.

[53] V. Yonten, M. Tanyol, N. Yildirim, N. C. Yildirim, and M. Ince, "Optimization of Remazol Brilliant Blue R dye removal by novel biosorbent P. eryngii immobilized on Amberlite XAD-4 using response surface methodology," *Desalination and Water Treatment*, vol. 57, no. 33, pp. 15592–15602, 2016.

[54] V. Yonten, H. Alp, N. Yildirim, N. C. Yildirim, and A. Ogedey, "Investigation of optimum conditions for efficient COD reduction in synthetic sulfamethazine solutions by Pleurotus eryngii var. ferulae using response surface methodology," *Journal of the Taiwan Institute of Chemical Engineers*, vol. 80, pp. 349–355, 2017.

[55] L. P. Lingamdinne, J. R. Koduru, Y. Y. Chang, and R. R. Karri, "Process optimization and adsorption modeling of Pb (II) on nickel ferrite-reduced graphene oxide nano-composite," *Journal of Molecular Liquids*, vol. 250, pp. 202–211, 2018.


The Scientific
World Journal
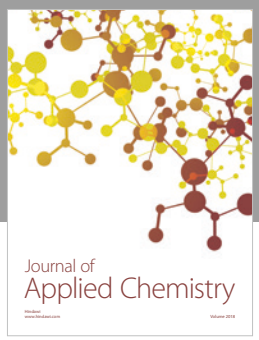
Journal of
Applied Chemistry
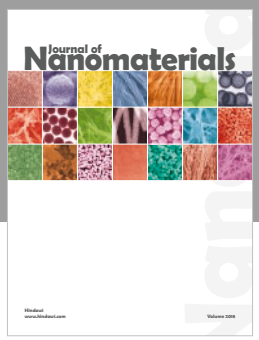
Journal of
Nanomaterials

Scientifica

International Journal of
Polymer Science
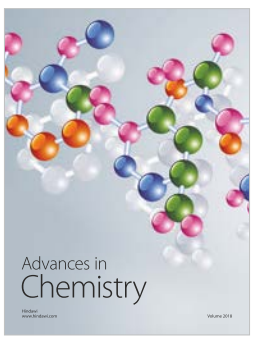
Advances in
Chemistry

Hindawi
Submit your manuscripts at
www.hindawi.com
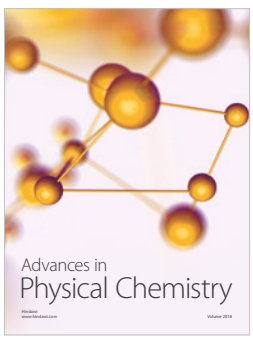
Advances in
Physical Chemistry

International Journal of
Analytical Chemistry
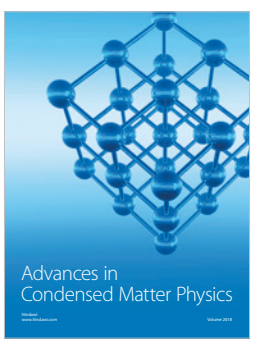
Advances in
Condensed Matter Physics
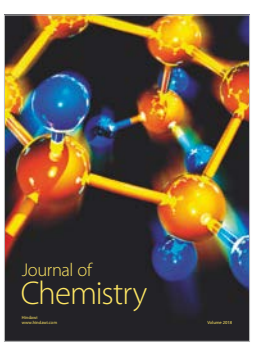
Journal of
Chemistry

International Journal of
Biomaterials
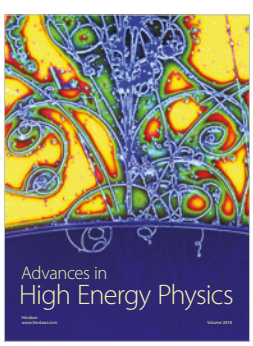
Advances in
High Energy Physics

Journal of
Engineering

Journal of
Nanotechnology

International Journal of
Corrosion

Journal of
Materials

BioMed
Research International
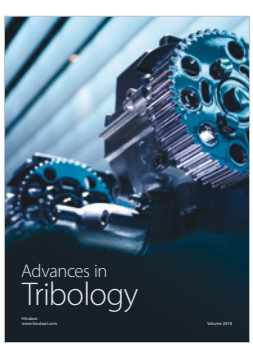
Advances in
Tribology
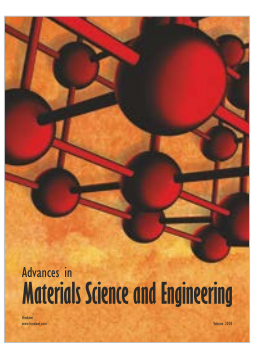
Advances in
Materials Science and Engineering